Subtropical estuarine carbon budget under various hydrologic extremes and implications on the lateral carbon exchange from tidal wetlands

Hongming Yao[1,#], Paul A. Montagna[2], Michael S. Wetz[2], Cory J. Staryk[2], and Xinping Hu[2,*]

[1]Department of Physical and Environmental Sciences, Texas A&M University-Corpus Christi, Texas 78412, United States

[2]Harte Research Institute for Gulf of Mexico Studies, Texas A&M University-Corpus Christi, Texas 78412, United States

[*]Corresponding author:

Xinping Hu (xinping.hu@tamucc.edu)

Current address:
Shenzhen Engineering Laboratory of Ocean Environmental Big Data Analysis and Application, Shenzhen Institute of Advanced Technology, Chinese Academy of Sciences, Shenzhen 518055, China

Highlights:

- Estuarine carbon fluxes are highly dynamic from drought to hurricane-induced flood.
- Lateral exchanges from tidal wetlands dominate the total carbon loading.
- Annual CO_2 emission from northwest Gulf of Mexico estuaries is double of the North American estuaries average.
- Interpretation of estuarine carbon budget requires greater spatiotemporal coverage to face the future climate change challenge.

Abstract

As coastal areas become more vulnerable to climatic impacts, the need for understanding estuarine carbon budgets with sufficient spatiotemporal resolution arises. Under various hydrologic extremes ranging from drought to hurricane-induced flooding, a mass balance model was constructed for carbon fluxes and their variabilities in four estuaries along the northwestern Gulf of Mexico (nwGOM) coast over a four-year period (2014–2018). Loading of total organic carbon (TOC) and dissolved inorganic carbon (DIC) to estuaries included riverine discharge and lateral exchange from tidal wetlands. The lateral exchanges of TOC and DIC reached 4.5 ± 5.7 and 8.9 ± 1.4 mol•C•m^{-2}•yr^{-1}, accounting for 86.5% and 62.7% of total TOC and DIC inputs into these estuaries, respectively. A relatively high regional CO_2 efflux (4.0 ± 0.7 mol•C•m^{-2}•yr^{-1}) was found, which was two times the average value in North American coastal estuaries reported in the literature. Oceanic export was the major pathway for losses of TOC (5.6± 1.7 mol•C•m^{-2}•yr^{-1}, 81.2% of total) and DIC (9.9 ± 2.9 mol•C•m^{-2}•yr^{-1}, 69.7% of total). The carbon budget exhibited high variability in response to hydrologic changes. For example, storm or hurricane induced flooding elevated CO_2 efflux by 2–10 times in short periods of time. Flood following a drought also increased lateral TOC exchange (from -3.5 ± 4.7 to 67.8 ± 17.6 mmol•C•m^{-2}•d^{-1}) but decreased lateral DIC exchange (from 28.9 ± 3.5 to -7.1 ± 7.6 mmol•C•m^{-2}•d^{-1}). The large variability of carbon budgets highlights the importance of high-resolution spatiotemporal coverage under different hydrologic conditions, and the importance of carbon contribution from tidal wetlands to coastal carbon cycling.

1 Introduction

Coastal areas consisting of tidal wetlands and estuaries play a crucial role in the global carbon cycle. Attempts to synthesize estuarine carbon budgets must deal with its high spatiotemporal heterogeneity that is due to geomorphological, climatic, and hydrologic differences (Bauer et al., 2013). More importantly, the lack of direct observations creates challenges with identifying exchange between tidal wetlands and estuarine waters (Najjar et al., 2018), even though a broad consensus regarding tidal wetlands' significance on estuarine carbon processing has recently emerged (Maher et al., 2018; Santos et al, 2021).

Generally, tidal wetlands transport carbon through lateral exchange including tidal activities and submarine groundwater discharge (Santos et al, 2021). Thus, a sufficient spatiotemporal resolution is needed to constrain these non-point source-driven exchanges (Santos et al., 2019; Tamborski et al., 2021). However, comprehensive budgets that combine organic and inorganic carbon fluxes over annual or longer timescales have been scarce (Bogard et al., 2020). Although wet–dry climatic cycles have been reported to alternate estuarine systems between heterotrophy and autotrophy (Yao et al., 2020), the variability of the coastal carbon cycle in response to hydrologic change remains understudied. All climate models predict the high possibility of hydrologic extremes, e.g., drought and flooding, in tropical and subtropical estuaries (Liu et al., 2019; Sherwood and Fu, 2014). Therefore, elucidating carbon budget variability spanning a full hydrologic spectrum is important to improve our knowledge and predict responses to future climate change.

Carbon fluxes can be estimated in several different ways. Process-based models that couple estuarine hydrodynamics and biogeochemistry can link organic and inorganic carbon cycles (Gordon et al., 1996). However, detailed information at fine spatial and temporal scales is required to constrain potential errors in these models (Bauer et al., 2013; Kemp et al., 1997). On the other hand, mass balance approaches based on observations and stoichiometric relationships may amplify uncertainties because of the propagation of errors (Smith et al., 1991). Nevertheless, models based on the latter approach can separate individual processes that significantly influence the regional carbon cycle, and errors could be constrained or at least recognized if temporal and spatial patterns are chosen carefully (Maher and Eyre, 2012).

There are few carbon budget estimates in subtropical estuaries worldwide (Crosswell et al., 2017; Maher and Eyre, 2012; Tanner and Eyre, 2020). The northwestern Gulf of Mexico (nwGOM) has the world's largest lagoonal estuary (Laguna Madre of both Texas, U.S.A. and Tamaulipas, Mexico) and many other smaller lagoonal estuaries (Dürr et al., 2011), i.e., estuaries that are separated from the coastal ocean by barrier islands, through which channels and waterways connect the water bodies. On the nwGOM coast, river discharge (or inflow) decreases sharply southward, which is one of the most distinctive hydrologic features in this area (Montagna et al., 2013). Climate fluctuations between drought and flood periods further alter and drive the hydrologic conditions of this coastal region (Yao and Hu, 2017; Yao et al., 2020). Moreover, nwGOM coast has a long history of hurricane landfalls (Roth, 2010). Through studying these estuarine systems that share geomorphological similarities, it is possible to assess the effects of hydrologic variations on the coastal carbon cycle and provide useful information for future climate change related investigations.

The objectives of this study were to: 1) construct comprehensive carbon budgets for nwGOM estuaries using a mass balance model based on bi-weekly (i.e., twice a month) to quarterly observations, 2) examine different biogeochemical drivers for processes including riverine inflow, lateral exchange, burial, air-water CO_2 flux, net ecosystem metabolism (NEM), and oceanic export, and 3) assess the climatic impact on the estuarine carbon budget, including alternating between drought and flood conditions.

2 Methods

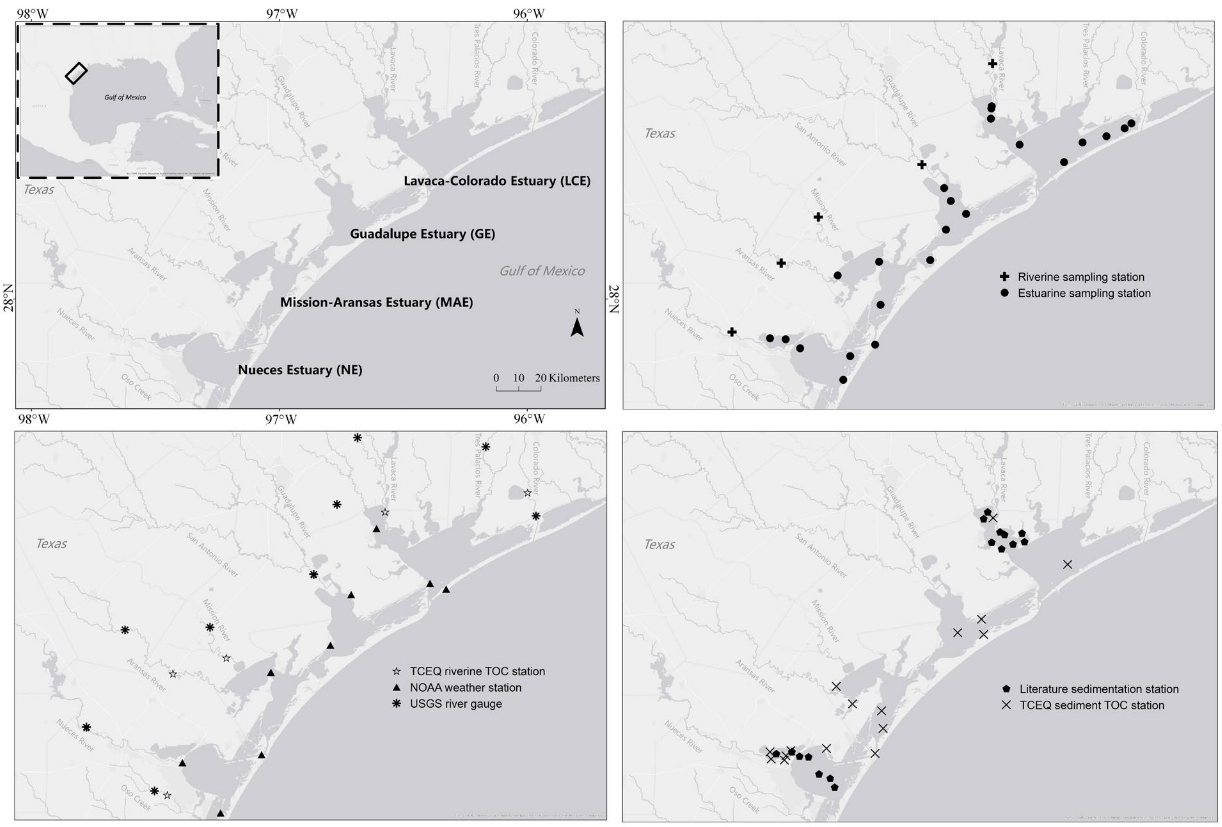

Figure 1. a, nwGOM estuaries names and locations. **b**, water column sampling stations. **c**, riverine and weather stations used in data interpretation. **d**, sedimentation stations used in data interpretation.

2.1 Study sites

Four nwGOM estuaries (Fig. 1a) — Lavaca-Colorado Estuary (LCE), Guadalupe Estuary (GE), Mission-Aransas Estuary (MAE), and Nueces Estuary (NE) — were investigated from April 2014 to April 2018. Average depth of these microtidal estuaries is approximately 1 m (Table 1), and these estuaries have restricted connections to the nwGOM due to the presence of a series of barrier islands (Fig. 1). Each estuary receives input from one or two rivers. We designated the upper estuary as the area subject to more freshwater influence from rivers, whereas the lower estuary represents the area connected with the nwGOM through a tidal inlet. The only exception was GE, which is river inflow-dominated due to its limited tidal exchange (Fig. 1) (Montagna and Kalke, 1992). Hurricane Harvey, a Category 4 storm, made landfall near the southern end of this coastal area on 25 August 2017 (Walker et al., 2021).

2.2 Field sampling and laboratory analyses

Field campaigns on different intervals were conducted (Table A1); both surface (0.1 m) and bottom samples (about 0.1 m above the bottom sediment) were taken. *In-situ* data, including temperature, depth, salinity, dissolved oxygen and chlorophyll-*a*, were acquired by a calibrated YSI 6600 V2 data sonde. pH, and dissolved inorganic carbon (DIC), total organic carbon (TOC), Ca^{2+}, and salinity were analyzed in the lab (see detailed analytical methods in Table A2). All pH measurements were conducted at 25 ± 0.1 °C, and the lab–measured pH values were converted to the total scale at *in-situ* temperature using CO2SYS with DIC and lab-measured pH as the input variables following the method in Yao and Hu (2017). To assess the estuarine carbon budget variability, we categorized the wide hydrologic range into four study periods: drought (D) and flood relaxation (FR) that both were under dry condition, flooding (F) and post-hurricane (H) that both were under wet condition. Hydrologic definitions are based on the quartiles of mean salinities (more details in Table A3). The only exception was the hurricane period, which included the post-storm surge period from September to early October 2017.

2.3 Carbon mass balance

The major carbon fluxes in an estuary involve multiple processes, including riverine input (F_{Rv}), net lateral exchange (F_L, including DIC and TOC), NEM (F_{NEM}), net CO_2 efflux (F_{CO2}), carbon deposition due to precipitation (F_P), oceanic export (F_{Ex}, i.e. net export after budgeting exchanging and residual flows between estuary and the coastal ocean, including DIC and TOC), sedimentation (F_D) and calcification (F_{Ca}). Consistent with other similar estuaries studies (Crosswell et al., 2017; Maher and Eyre, 2012; Tanner and Eyre, 2020), a steady-state assumption was made for the nwGOM estuaries. The steady-state mass balance equation for estuarine DIC can be written as:

$$F_{Rv-DIC} + F_{L-DIC} + F_{P-DIC} = F_{NEM} + F_{CO2} + F_{Ca} + F_{Ex-DIC} \quad (1)$$

F_{NEM} is negative for heterotrophy and positive for autotrophy. For total organic carbon, which consists of dissolved organic carbon (DOC) and particulate organic carbon (POC), the steady-state equation can be written as:

$$F_{Rv-TOC} + F_{L-TOC} + F_{P-TOC} + F_{NEM} = F_D + F_{Ex-TOC} \quad (2)$$

Note that all budget terms are estimated independently except for the lateral exchange ones, which are calculated as the residuals from the two mass balance equations.

2.4 Riverine input (F_{Rv})

Riverine carbon fluxes (F_{Rv}, $\mu mol \cdot C \cdot d^{-1}$) were estimated from riverine DIC and TOC concentrations (C_{Rv}, $\mu mol \cdot C \cdot kg^{-1}$), daily average discharge (V_{Rv}, $m^3 \cdot d^{-1}$; Table 1) and water density (ρ, $kg \cdot m^{-3}$):

$$F_{Rv} = C_{Rv} \times V_{Rv} \times \rho \quad (3)$$

where riverine DIC was estimated from our bimonthly surveys at upstream of river mouths between October 2015 and May 2018 (see Fig. 1b for station information; Table 1 for averaged endmember values; Table A1 for sampling schedule), and riverine TOC were retrieved from discrete data (2004 – 2018, Table A4 for sampling schedule) collected by the Surface Water Quality Monitoring Program (SWQM) of Texas Commission on Environmental Quality (TCEQ; https://www.tceq.texas.gov/waterquality/monitoring/index.html). Average riverine DIC and TOC were derived from dry and wet conditions (see values in Table 1, hydrologic condition categorization in Table A3), respectively. Cumulative monthly discharges were obtained from gauges of the U.S. Geological Survey (USGS; https://waterdata.usgs.gov/tx/nwis/rt) (Fig.1c; Table 1).

2.5 Precipitation (F_P)

Carbon deposition through precipitation was assessed for TOC and DIC, respectively. Regional atmospheric POC deposition was small enough ($0.1 – 1.3\times10^{-3}$ μmol·C·L^{-1} , Benway and Coble, 2014) to be omitted in the budget calculations. Average atmospheric DOC (440 μmol·C·L^{-1}; Mitra et al., 2017) and DIC (17 μmol·C·L^{-1}; Willey et al., 2000) concentrations were used in conjunction with monthly precipitation rate (Texas Water Development Board or TWDB, http://www.twdb.texas.gov/) to estimate rainfall input of carbon to these estuaries.

2.6 Air-water CO_2 flux (F_{CO2})

The net CO_2 flux (F_{CO2}; mmol·C·m^{-2}·d^{-1}) at each station was calculated using Eq. 4 (see method in Table A5):

$$F_{CO2} = k \cdot K_0(p\mathrm{CO}_{2,\mathrm{water}} - p\mathrm{CO}_{2,\mathrm{air}}) \qquad (4)$$

where K_0 was solubility coefficient calculated from temperature and salinity (mol·C·m^{-3}·Pa^{-1}; Weiss, 1974), k was the gas transfer velocity that was derived from daily average wind speed at 10 m height (cm·h^{-1}; Jiang et al., 2008) and $p\mathrm{CO}_{2,\mathrm{air}}$ (μatm) was partial pressure of atmospheric CO_2. $p\mathrm{CO}_{2,\mathrm{water}}$ (μatm) was calculated using measured DIC (± 0.1%) and pH (± 0.0004 or ± 0.01 depending on the analytical method used) as the input variables and the program CO2SYS. Calculated $p\mathrm{CO}_{2,\mathrm{water}}$ values were in good agreement with *in-situ* monitored $p\mathrm{CO}_{2,\mathrm{water}}$ measurements (± 20 μatm; McCutcheon et al., 2021).

2.7 Net ecosystem metabolism (F_{NEM})

Because mixed layer benthic and pelagic metabolic processes would generate/consume CO_2 and influence F_{CO2} directly, NEM was estimated using a linear regression equation (Eq. 5) derived by Maher and Eyre (2012). They found a significant inverse relationship ($R^2 = 0.898$, $p < 0.001$) between F_{CO2} and F_{NEM} based on data from 12 estuaries worldwide. Laruelle et al. (2013) further applied this equation to estimate another 68 lagoonal estuarine F_{CO2} globally and suggested ~26.8% difference between directly calculated CO_2 flux and NEM-derived estimates. Here, we calculated daily NEM at each station following the same equation:

$$F_{CO2} = -0.4236 \times F_{NEM} + 11.991 \qquad (5)$$

2.8 Sediment deposition (F_D)

Sediment deposition flux (F_D; mmol·C·m^{-2}·d^{-1}) was determined by sedimentation rates (S_a, cm·yr^{-1}), sedimentary TOC concentrations (C_{sed}; mg·C·kg^{-1}) and averaged dry bulk sediment density (0.88 g·cm^{-3}) in nwGOM estuaries calculated the linear sediment accumulation rates (Table 1):

$$F_D = S_a \times C_{sed} \times \rho_s \qquad (6)$$

Due to the invariant ^{210}Pb profiles in the well mixed upper layer of these shallow estuaries (20-cm cores from our campaigns, D. Hammond, pers. Comm.), we chose to use the average sediment accumulation rates in Lavaca Bay (upper LCE) and NE to represent those in GE and MAE, respectively (Bronikowski, 2004; Yeager et al. 2006) (Table 1). In addition, historical surface sedimentary TOC data were obtained from TCEQ and averaged for dry and wet conditions (Table 1) with slight mismatch due to sampling time inconsistencies between TCEQ surveys and our study. Thus, averaged sedimentation rates under dry and wet conditions were applied to corresponding upper and lower estuarine systems.

2.9 Oceanic export (F_{EX})

Due to shallow and windy conditions, the estuarine water was assumed to be well mixed (little stratification was observed during our study period). A box-modeling approach was then introduced to estimate the F_{EX}. The steady-state net daily average F_{EX} was calculated based on the Land-Ocean Interactions in the Coastal Zone method (LOICZ; Smith et al., 2005):

$$\left.\begin{aligned} V_R &= V_{Rv} + V_{SGD} + V_P - V_E \\ V_X &= \frac{V_R \times S_R}{\mathrm{S}_{ocean} - \bar{\mathrm{S}}} \\ F_{Ex} &= V_R \times C_R + V_X \times (\bar{\mathrm{C}} - C_{ocean}) \end{aligned}\right\} \quad (7)$$

V_R ($m^3 \cdot d^{-1}$) was the residual freshwater flow between the system and the adjacent open ocean, V_{Rv} was daily river discharge, V_{SGD} was annual mean SGD from the literature (Table 1), note that we assumed most SGD occurred within 50 m from the shoreline in upper estuaries according to Spruill and Bratton (2008); V_P and V_E denoted precipitation and evaporation volume (see in Section 2.5), V_X was exchange flow between an estuary and adjacent coastal ocean (negative sign denotes export to the coastal ocean, positive sign denotes net import), $\bar{\mathrm{S}}$, S_R, S_{ocean} were the salinities from system-averaged, ocean-estuary boundary, ocean endmember, respectively; $\bar{\mathrm{C}}$, C_R, C_{ocean} were system-averaged, ocean-estuary boundary, ocean endmember DIC or TOC values, respectively (more details in Table 1).

2.10 Calcification (F_{Ca})

Daily calcification rates were calculated as the difference of measured Ca^{2+} concentrations (Ca_i^{2+}, $mmol \cdot kg^{-1}$) and salinity-normalized Ca^{2+} (nCa_i^{2+}, $mmol \cdot kg^{-1}$) from each sampling campaign:

$$\left.\begin{aligned} nCa_i^{2+} &= \frac{(\mathrm{Sal}_{ocean} - \mathrm{Sal}_i) \times Ca_{river}^{2+} + (\mathrm{Sal}_i - \mathrm{Sal}_{river}) \times Ca_{ocean}^{2+}}{\mathrm{Sal}_{ocean} - \mathrm{Sal}_{river}} \\ F_{Ca} &= Ca_i^{2+} - nCa_i^{2+} \end{aligned}\right\} \quad (8)$$

Sal was salinity, subscript *i* denoted the *i*-th campaign, subscript *river* and *ocean* denote the two endmembers values, respectively; positive F_{Ca} indicated calcification and negative indicates carbonate dissolution.

2.11 Lateral exchange (F_L)

Lateral exchange of DIC and TOC were the only unknown terms and were calculated as residuals from Eqs. 1 and 2, respectively. Positive values indicate the flux direction from tidal wetlands to estuarine water, whereas negatives denote the opposite direction.

2.12 Estuarine area normalized annual fluxes

Finally, the annual fluxes of different carbon budget terms were averaged by the sum of all campaigns, and normalized to corresponding estuarine areas for further comparison:

$$\left.\begin{aligned} \overline{F_i} &= \frac{\overline{F_i^{up}} \times S_{up} + \overline{F_i^{low}} \times S_{low}}{S_{up} + S_{low}} \\ F_x &= \frac{\sum_1^i (\overline{F_i} \times d_i)}{\sum_1^i d_i} \end{aligned}\right\} \quad (9)$$

$\overline{F_i^{up}}$ and $\overline{F_i^{low}}$ (mmol·C·d^{-1}) were arithmetic means of carbon fluxes in upper and lower estuaries from campaign *i*, S_{up} and S_{low} were upper and lower estuary surface areas in individual estuaries, $\overline{F_i}$ (mmol·C·m^{-2}·d^{-1}) was area-normalized average flux in campaign *i*, d_i was the duration (days) between two consecutive sampling campaigns, F_x (mol·C·m^{-2}·yr^{-1}) denoted the area- normalized annual flux of carbon budget term *x* (including all terms above).

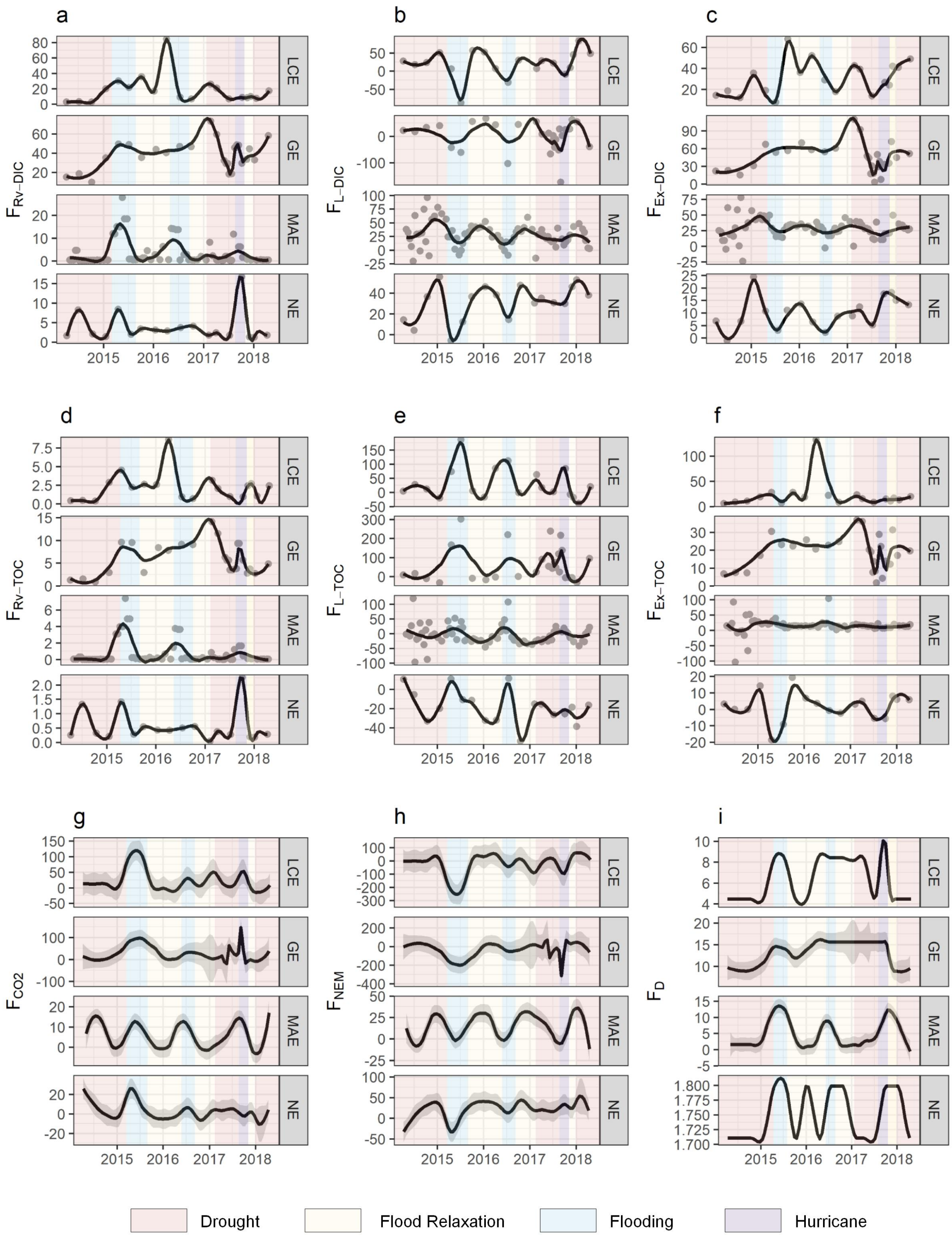

Figure 2. Observed or modeled carbon fluxes in four estuaries, shaded areas denote the 95% confidence level based on locally weighted least squares regression (loess). (unit: $mmol{\cdot}C{\cdot}m^{-2}{\cdot}d^{-1}$)

3 Results

3.1 Riverine input

Average river discharge ranged from 107.9 ± 19.7 $m^3 \cdot s^{-1}$ (hereafter the uncertainties were all standard errors) in northern estuary LCE to 8.6 ± 2.4 $m^3 \cdot s^{-1}$ in southern estuary NE, consistent with the declining trend of inflow (Table 1). Distinct seasonality was observed with high river discharge in spring and summer in response to storm-driven flooding in 2015, 2016 and 2017; but fall and winter had much less discharge. As a result, $F_{Rv\text{-}DIC}$ and $F_{Rv\text{-}TOC}$ had similar seasonal patterns but different magnitudes (Figs. 2a and 2d). During the spring to summer flooding period, maximum $F_{Rv\text{-}DIC}$ in LCE and GE reached 84.4 and 59.5 $mmol \cdot C \cdot m^{-2} \cdot d^{-1}$, respectively, while those in MAE and NE were substantially lower (27.8 and 16.7 $mmol \cdot C \cdot m^{-2} \cdot d^{-1}$, respectively). Similarly, maximum $F_{Rv\text{-}TOC}$ were 8.6 and 14.1 $mmol \cdot C \cdot m^{-2} \cdot d^{-1}$ for LCE and GE, respectively; compared to 7.4 and 2.3 $mmol \cdot C \cdot m^{-2} \cdot d^{-1}$ for MAE and NE, respectively.

3.2 Air-water CO_2 flux

All four estuaries were net CO_2 sources to the atmosphere (Fig. 3) with distinct spatiotemporal patterns (Fig. 2g), F_{CO2} ranged -15 – 120 $mmol \cdot C \cdot m^{-2} \cdot d^{-1}$. In spring and summer, these estuaries had higher CO_2 emission (up to 120 $mmol \cdot C \cdot m^{-2} \cdot d^{-1}$) as a result of flooding (Yao and Hu 2017; Yao et al., 2020). The peak of CO_2 efflux values in LCE and GE (~100 $mmol \cdot C \cdot m^{-2} \cdot d^{-1}$) were five times of those in MAE and NE (~20 $mmol \cdot C \cdot m^{-2} \cdot d^{-1}$) (Fig. 2g). Maximum CO_2 efflux occurred when the first major storm struck at the end April 2015 after a four-year extreme drought (Yao and Hu, 2017). In comparison, F_{CO2} decreased and even changed sign (-15 – 35 $mmol \cdot C \cdot m^{-2} \cdot d^{-1}$) in fall and winter. Nevertheless, average CO_2 flux in LCE and GE (~10 $mmol \cdot C \cdot m^{-2} \cdot d^{-1}$) under this low freshwater conditions was ten times of MAE and NE average (~1 $mmol \cdot C \cdot m^{-2} \cdot d^{-1}$). Overall, annual average F_{CO2} in LCE and GE was one order of magnitude higher than those in MAE and NE (Fig. 3).

3.3 NEM

Derived from F_{CO2} empirically, the F_{NEM} variations were anticorrelated with the F_{CO2} pattern. The F_{NEM} values were lowest in spring and summer (0.5 ± 5.6 and -27.7 ± 10.9 mmol·C·m^{-2}·d^{-1}; respectively), indicating the seasonal heterotrophy. Increasing NEM in fall (7.5 ± 7.4 mmol·C·m^{-2}·d^{-1}) and winter (35.5 ± 3.5 mmol·C·m^{-2}·d^{-1}) showed switching to autotrophic conditions. Annual F_{NEM} values suggested heterotrophic dominance in the northern estuaries (i.e., LCE and GE), whereas yearly autotrophy was found in the southern estuaries, MAE and NE (Fig. 3).

3.4 Sediment deposition

Annual average sediment organic carbon deposition flux F_D was 2.3 ± 0.2 mol·C·m^{-2}·yr^{-1} in LCE, with 1.9 ± 0.2 and 3.1 ± 0.1 mmol·C·m^{-2}·d^{-1} in dry and wet conditions, respectively. F_D was the highest in GE at 4.7 ± 0.2 mol·C·m^{-2}·yr^{-1}, 4.8 ± 0.2 mmol·C·m^{-2}·d^{-1} in dry and 5.7 ± 0.1 mmol·C·m^{-2}·d^{-1} in wet conditions. Then F_D declined toward the south (averaged 1.7 ± 0.2 mol·C·m^{-2}·yr^{-1}, with 1.2 ± 0.2 mol·C·m^{-2}·yr^{-1} in dry and 4.6 ± 0.1 mol·C·m^{-2}·yr^{-1} in wet in MAE; and averaged 0.6 ± 0.1 mol·C·m^{-2}·yr^{-1} , with 0.6 ± 0.1 mol·C·m^{-2}·yr^{-1} in dry and 0.7 ± 0.1 mol·C·m^{-2}·yr^{-1} in wet in NE, Figs. 2i & 3).

3.5 Export to the coastal ocean

Area-normalized $F_{Ex\text{-}DIC}$ was between -24 – 109 mmol·C·m^{-2}·d^{-1}, and $F_{Ex\text{-}TOC}$ was -103 – 132 mmol·C·m^{-2}·d^{-1} in all estuaries combined (Figs. 2c and 2f). The highest monthly $F_{Ex\text{-}DIC}$ and $F_{Ex\text{-}TOC}$ were both found in GE (February 2017) and in LCE (April 2016), respectively. Occasional negative $F_{Ex\text{-}DIC}$ in MAE and NE indicated a possible oceanic water supply under drought conditions when riverine inputs were low (to compensate for evaporative water loss). Consistent with river inflows, these estuaries exported most DIC and TOC to the GOM in winter and spring

(38.6 ± 4.1 and 19.2 ± 3.7 $mmol\cdot C\cdot m^{-2}\cdot d^{-1}$, respectively). Coastwide minimum $F_{Ex\text{-}DIC}$ occurred in summer (20.6 ± 2.5 $mmol\cdot C\cdot m^{-2}\cdot d^{-1}$) and minimum $F_{Ex\text{-}TOC}$ in fall (11.3 ± 2.9 $mmol\cdot C\cdot m^{-2}\cdot d^{-1}$), during which time minimum $F_{Ex\text{-}DIC}$ ranged from 2.4 ± 1.3 (NE) to 32.4 ± 6.0 (GE) $mmol\cdot C\cdot m^{-2}\cdot d^{-1}$; minimum $F_{Ex\text{-}TOC}$ fluctuated between 2.8 ± 5.6 (NE) and 16.9 ± 5.9 (GE) $mmol\cdot C\cdot m^{-2}\cdot d^{-1}$. Among the annual F_{Ex} values, DIC export from southern estuary NE (3.5 ± 0.5 $mol\cdot C\cdot m^{-2}\cdot yr^{-1}$) was found to be only ~1/5 of the northern estuary GE (17.5 ± 1.7$mol\cdot C\cdot m^{-2}\cdot yr^{-1}$); similarly, lowest annual TOC export was found in NE (0.6 ± 0.7 $mol\cdot C\cdot m^{-2}\cdot yr^{-1}$, Fig. 3).

3.6 Lateral exchange

Although average DIC and DOC fluxes due to SGD in upper NE (~4050 and 840 $mmol\cdot C\cdot m^{-2}\cdot d^{-1}$, respectively) has been estimated from a previous study (Murgulet et al., 2018), these overwhelmingly high carbon inflows should diminish toward lower estuary so that can be balanced by much lower estuarine carbon export (Sections 3.2, 3.4 and 3.5). Due to possible error amplification from limited data coverage, lateral exchanges were calculated as the residual term from the mass balance models (Eqs. 1 & 2) rather than the SGD study directly.

Area-normalized $F_{L\text{-}DIC}$ ranged from -173.1 – 96.0 $mmol\cdot C\cdot m^{-2}\cdot d^{-1}$, and $F_{L\text{-}TOC}$ ranged -96.2 – 301.6 $mmol\cdot C\cdot m^{-2}\cdot d^{-1}$ (Figs. 2b & 2e). The southern estuaries (MAE and NE) had the higher annual $F_{L\text{-}DIC}$, while larger annual $F_{L\text{-}TOC}$ were found in the northern estuaries (LCE and GE), respectively (Fig. 3). Four-estuary averaged $F_{L\text{-}DIC}$ reached the maximum (48.0 ± 3.8 $mmol\cdot C\cdot m^{-2}\cdot d^{-1}$) and minimum (0.6 ± 5.5 $mmol\cdot C\cdot m^{-2}\cdot d^{-1}$) values in winter and summer, respectively, by contrast $F_{L\text{-}TOC}$ varied in the opposite direction (maximum 39.8 ± 12.8 $mmol\cdot C\cdot m^{-2}\cdot d^{-1}$ in summer and minimum -20.2 ± 4.2 $mmol\cdot C\cdot m^{-2}\cdot d^{-1}$ in winter) (Figs. 2b & 2e).

3.7 Carbon budget

The annual carbon budget in each estuary was calculated by the area-integrated DIC and TOC fluxes (Fig. 3). The largest DIC input was $F_{L\text{-}DIC}$. In particular, $F_{L\text{-}DIC}$ in NE was estimated to be almost ten times of $F_{Rv\text{-}DIC}$. On the other hand, F_{CO2} and $F_{Ex\text{-}DIC}$ were two major DIC loss pathways from nwGOM estuaries, in addition autotrophic activities appeared to be another important DIC loss term in southern estuaries MAE and NE. On the organic carbon side, the four-estuary averaged $F_{L\text{-}TOC}$ was the major total TOC input, which was almost seven times of $F_{Rv\text{-}TOC}$ in this region. In addition, annual NEM revealed varying trophic status from heterotrophy to autotrophy when moving southward. $F_{Ex\text{-}TOC}$ contributed ~75% of total TOC outflow, but behaved differently among these four subsystems. F_D was another important TOC loss term, which was estimated to account for the remaining 25% of total TOC outflow. Compared to the above fluxes, F_P and F_{Ca} were small enough so that they were omitted in the overall budget (Fig. 3).

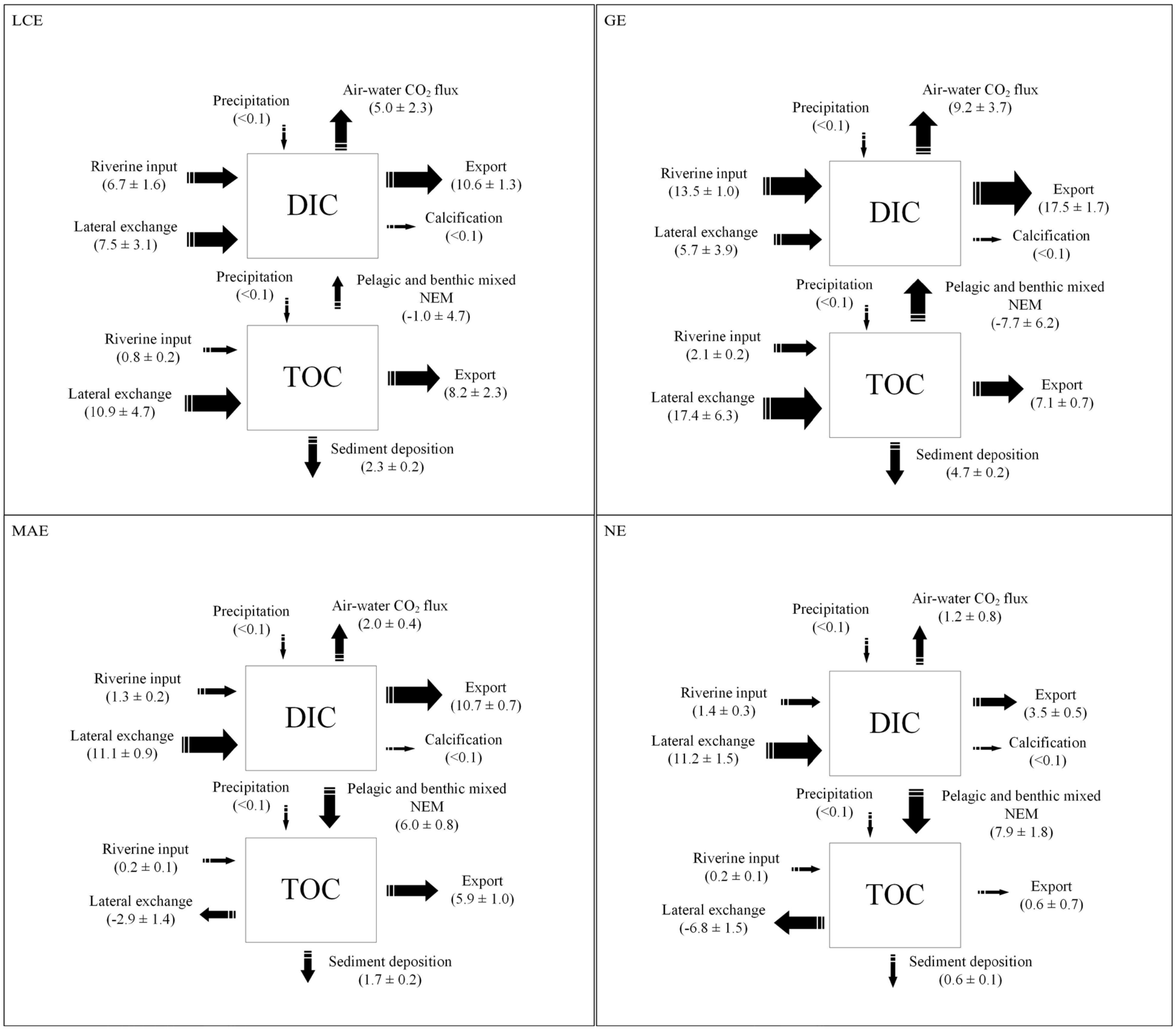

Figure 3. Carbon fluxes for DIC and TOC in the four studied estuaries, "±" indicates standard deviation. (unit: $mmol{\cdot}C{\cdot}m^{-2}{\cdot}d^{-1}$)

4 Discussion

4.1 Hydrologic controls on estuarine carbon budgets

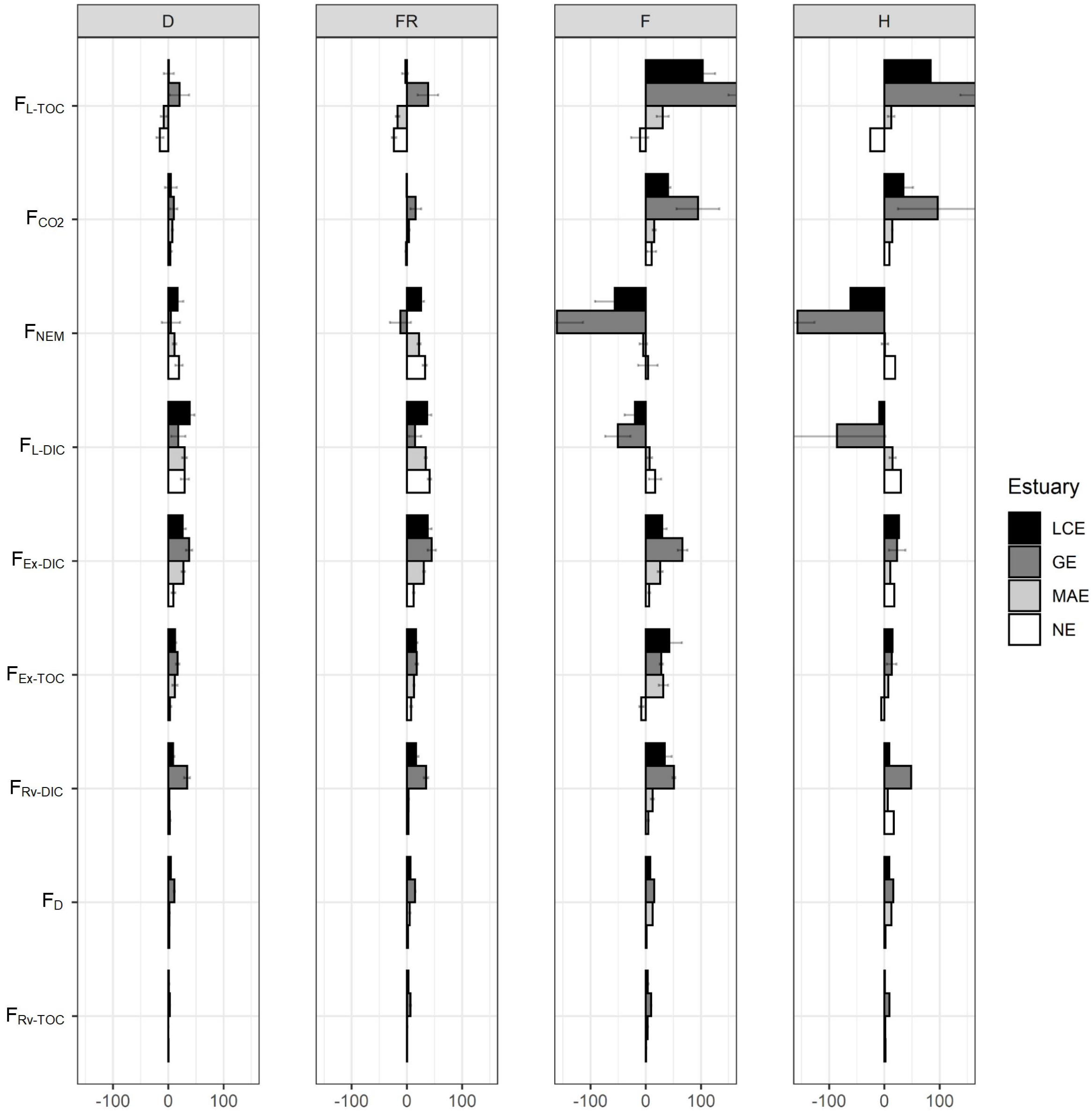

Figure 4. Carbon fluxes under different hydrologic conditions in the four studied estuaries. The headings represent D = drought; FR = flood relaxation; F = flooding; H = hurricane. For better comparison and visualization, few columns exceed x-axis limit and are not fully displayed. (unit: $mmol{\cdot}C{\cdot}m^{-2}{\cdot}d^{-1}$)

During our study period, the nwGOM coast experienced extreme hydrologic changes between dry and wet conditions, including the end of extreme drought (prior to April 2015) and a

Category 4 storm (Hurricane Harvey in fall 2017). . Both flooding and flood relaxation occurred at multiple periods over time. $F_{L\text{-}TOC}$, F_{CO2} and F_{NEM} experienced the largest changes across different periods (Fig. 4). F_{CO2} indicated large estuarine CO_2 emission rates (5.3 ± 2.7 – 44.3 ± 25.1 $mmol\cdot C\cdot m^{-2}\cdot d^{-1}$) across all conditions. Flooding from Hurricane Harvey increased F_{CO2} by 2 – 10 times compared to the baseline values, with most pronounced increase in LCE (4.5 ± 10.9 to 40.7 ± 4.1 $mmol\cdot C\cdot m^{-2}\cdot d^{-1}$) and GE (9.6 ± 6.7 to 96.7 ± 72.0 $mmol\cdot C\cdot m^{-2}\cdot d^{-1}$) compared to MAE (7.3 ± 1.3 to 15.4 ± 2.9 $mmol\cdot C\cdot m^{-2}\cdot d^{-1}$) and NE (3.8 ± 2.7 to 11.0 ± 8.2 $mmol\cdot C\cdot m^{-2}\cdot d^{-1}$) that had smaller increases. Two estuaries, MAE and NE, were on the "dry" side of the storm and riverine input did not substantially increase as shown by their lower $F_{Rv\text{-}DIC}$ and $F_{Rv\text{-}TOC}$ (Figs. 2a & 2d). This CO_2 flux increase in LCE and GE was consistent with other studies that also found 5 – 10 times elevation of estuarine CO_2 efflux due to either storms or storm-induced flooding (Crosswell et al., 2014; Van Dam et al., 2018; Hu et al., 2020). Such increase could be attributed to enhanced heterotrophy in response to discharge events (Russell et al., 2006) as well as riverine CO_2 ventilation (Yao et al., 2020). Walker et al. (2021) also found bottom hypoxia in GE after Hurricane Harvey in 2017. Similarly, $F_{Ex\text{-}DIC}$ and $F_{Rv\text{-}DIC}$ followed the F_{CO2} pattern (Fig. 4).

Our study assessed the hydrologic effect on lateral carbon exchange in nwGOM estuaries. As expected, storm- and hurricane-driven flooding increased $F_{L\text{-}TOC}$ from -3.5 ± 4.7 $mmol\cdot C\cdot m^{-2}\cdot d^{-1}$ (drought) to 72.6 ± 37.4 $mmol\cdot C\cdot m^{-2}\cdot d^{-1}$ (hurricane) (Figs. 4D to 4H), this enhanced exchange was most likely caused by large surface runoff (Walker et al., 2021). Because residence time is a key control on estuarine organic carbon degradation (Hopkinson et al., 1998), the moderate to long residence time in these four estuaries (39 – 360 d, Table 1), particularly in MAE and NE, was likely responsible for organic carbon processing, hence related carbon fluxes. These values indicate that storm-flushed organic matter from tidal wetland supported large estuarine heterotrophy and CO_2 emission in the wet condition, which further confirmed the crucial role of lateral exchange. In contrast, $F_{L\text{-}DIC}$ was found to decrease from 28.9 ± 3.5 $mmol \cdot C \cdot m^{-2} \cdot d^{-1}$ (drought) to -20.2 ± 31.1 $mmol \cdot C \cdot m^{-2} \cdot d^{-1}$ (hurricane) (Figs. 4D to 4H). This indicates increased DIC uptake at tidal wetland side under wet condition.

Russell et al. (2006) concluded that heterotrophic NEM in this region would not exceed -5 $mg \cdot O_2 \cdot l^{-1} \cdot d^{-1}$ (or -312.5 $mmol \cdot C \cdot m^{-2} \cdot d^{-1}$ based on the average depth of 1 m) by integrating open-water and benthic chamber results. Annually aggregated NEM (1.7 ± 3.5 $mol \cdot C \cdot m^{-2} \cdot yr^{-1}$) indicates a balance between primary production and remineralization coastwide, yet with a large range from heterotrophic northern estuaries to autotrophic southern estuaries (Fig. 3). However, the coastwide autotrophy during drought (11.8 ± 3.3 $mmol \cdot C \cdot m^{-2} \cdot d^{-1}$) and flood relaxation (15.1 ± 5.4 $mmol \cdot C \cdot m^{-2} \cdot d^{-1}$) periods could be attributed to benthic activities once DIC became more available while TOC decreased in the water column. For example, model simulation in Galveston Bay, about 200 km north of the study area, illustrated that oxygen concentration could quickly decrease to zero from ambient concentration in one hour without benthic photosynthesis (An and Joye, 2001). The nearly balanced NEM was comparable to other lagoonal estuaries. In New River Estuary of North Carolina, NEM was between -3.0 – 1.1 $mol \cdot C \cdot m^{-2} \cdot yr^{-1}$ (Crosswell et al., 2017), however its annual F_{CO2} (-0.2 – 2.0 $mol \cdot C \cdot m^{-2} \cdot yr^{-1}$) was only half of what we found in the nwGOM estuaries.

It is notable that similar magnitude of carbon budgets had been observed between flooding and hurricane periods (Figs. 4F and 4H). The comparable $F_{Rv\text{-}DIC}$, $F_{Rv\text{-}TOC}$, and $F_{L\text{-}TOC}$ were indicative of analogous terrestrial discharges, this could be reflected by the comparable salinities during these two periods (Table A3). Likely the storm pulses were followed by maximum discharge to estuary (Paerl et al., 2018). Such discharge should depend on the varying hydrology in each estuarine system and the connected watershed.

4.2 Importance of lateral exchange from tidal wetlands (saltmarsh and mangroves)

Tidal saltmarsh and mangrove systems are among the most productive ecosystems on Earth (Bouillon et al., 2008; Cai, 2011). In general, the major mechanisms that drive F_L between saltmarshes/mangroves and estuaries should include tidal exchange, SGD, eddy diffusion, and rain (Maher et al., 2018; Santos et al., 2019). However, their role in estuarine carbon cycle remains largely unsolved because of difficulties in making direct measurements. Previous studies showed wide ranges between 3.4 – 102.2 $mol \cdot C \cdot m^{-2} \cdot wetland \cdot yr^{-1}$ for $F_{L\text{-}TOC}$ and 11.9 – 177.0 $mol \cdot C \cdot m^{-2} \cdot wetland \cdot yr^{-1}$ for $F_{L\text{-}DIC}$; respectively (Table 2).

In the current study, annual F_{Rv} introduced only a small portion of total inputs (~13.5 % for TOC and ~37.3 % for DIC). By contrast $F_{L\text{-}TOC}$ was more than 6 times of $F_{Rv\text{-}TOC}$, $F_{L\text{-}DIC}$ was almost double of $F_{Rv\text{-}DIC}$. Given that the nwGOM coastline has an extensive distribution of saltmarshes and mangroves (nearly half of the entire U.S. East Coast, Table 2), previously overlooked tidal wetland systems may serve as an important carbon source to coastal waters in this semiarid area. If converted to tidal wetland yields (annual fluxes normalized to wetland area), $F_{L\text{-}TOC}$ and $F_{L\text{-}DIC}$ could reach 16.7 ± 21.4 and 33.5 ± 5.1 $mol \cdot C \cdot m^{-2} \cdot wetland \cdot yr^{-1}$. These values coincided with those from U.S. East Coast and Australia East Coast (Table 2), where riverine carbon became the dominance (67 ± 8% in U.S. East Coast; Najjar et al., 2018). Note that in river-dominated GE, ~70% of total DIC inputs were transported by river discharges. Consequently, carbon exchange in tidal wetland should be a focus of ocean-dominated estuary carbon budget studies.

Consistent with earlier studies (Wang et al., 2017; Chen et al., 2018), $F_{L\text{-}TOC}$ and $F_{L\text{-}DIC}$ in nwGOM estuaries also exhibited seasonal patterns (Figs. 2b & 2e), i.e., high $F_{L\text{-}TOC}$ but low $F_{L\text{-}DIC}$ in spring and summer as compared by low $F_{L\text{-}TOC}$ but high $F_{L\text{-}DIC}$ in winter. One explanation was a high DIC uptake due to the maximum plant growth rate in spring and summer for wetland system (Wang et al., 2017). Additionally, concurrent floods flushed more surface organic carbon from wetlands to estuaries (Walker et al., 2021). Whereas high DIC:DOC ratio SGD in winter favored high $F_{L\text{-}DIC}$ (Murgulet et al., 2018). However, given its large spatiotemporal variability, more detailed quantification of the lateral exchange is desired for future estuarine carbon budget studies.

F_{CO2} in these estuaries may be largely dependent on F_L ($p < 0.001$ for both $F_{L\text{-}TOC}$ and $F_{L\text{-}DIC}$ in Figs. 5a & b). While $F_{L\text{-}TOC}$ contributed significantly to F_{CO2} change coastwide (Fig. 5a), the effect of $F_{L\text{-}DIC}$ on F_{CO2} varied from one estuary to another. This was attributed to varying primary production in different estuaries as river input decreased to the southwest. This is indicated by the declining CO_2 emission or even occasional CO_2 uptake (Figs. 2g & 3), stronger autotrophy in southwestern estuaries MAE and NE was largely due to the limited riverine organic matter supply. Therefore, the significant inverse relationship between $F_{L\text{-}DIC}$ and F_{CO2} in MAE and NE (both $p < 0.001$; Fig. 5b) also indicates the potentially greater contribution on estuarine autotrophic activities from lateral exchange. Nevertheless, the close relationship between $F_{L\text{-}TOC}$ and F_{NEM} across four estuaries ($r = 0.924$, $N = 140$, $p < 0.001$; Fig. 5c) highlighted the significant support of tidal wetland on estuarine NEM, as $F_{Rv\text{-}TOC}$ was generally small overall (Fig. 3).

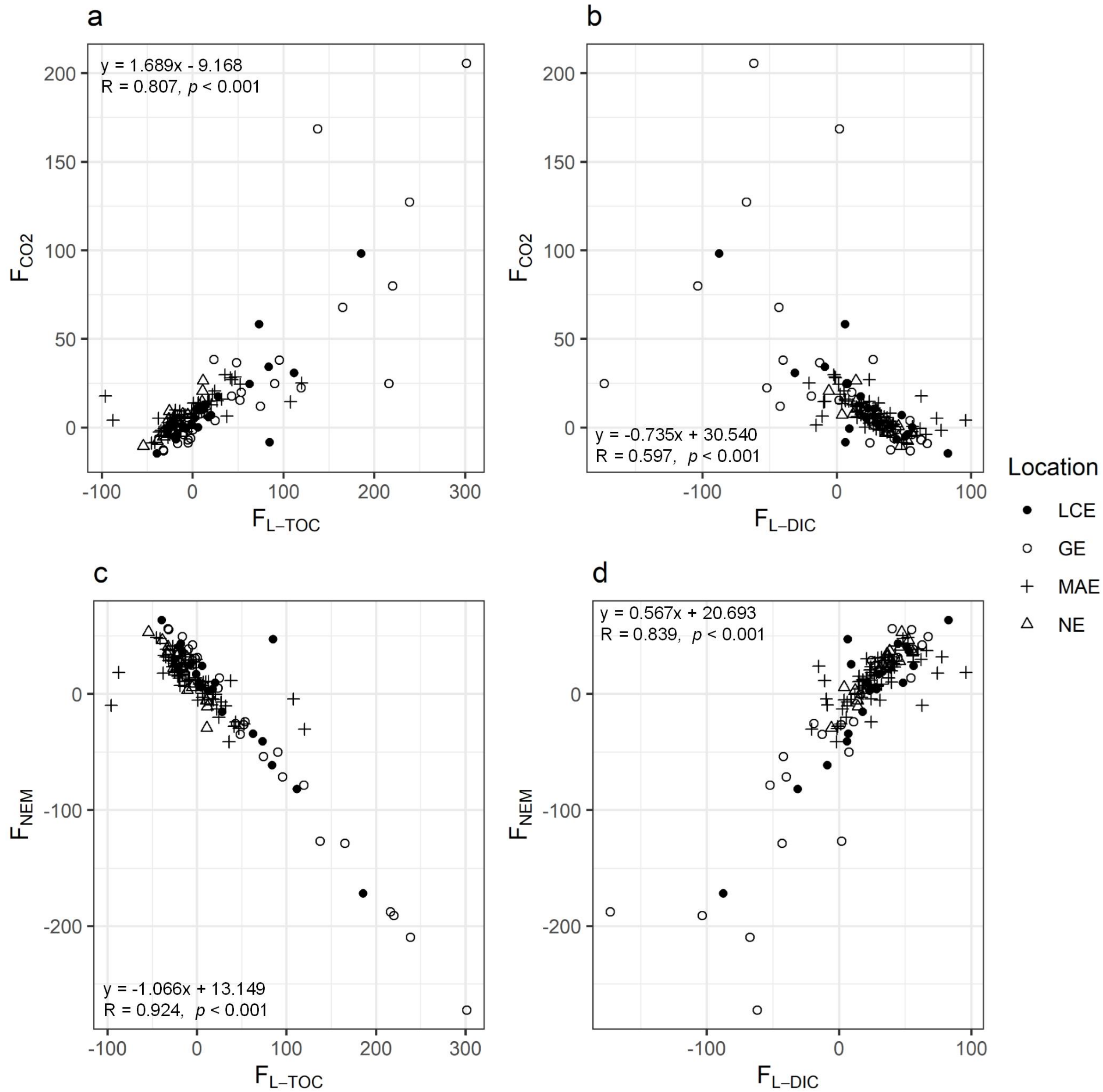

Figure 5. Relationships among different fluxes in four estuaries. **a**, lateral TOC vs. air-water CO_2 flux. **b**, lateral DIC vs. air-water CO_2 flux. **c**, lateral TOC vs. NEM. **d**, lateral DIC vs. NEM. (unit: $mmol \cdot C \cdot m^{-2} \cdot d^{-1}$)

4.3 Integrated carbon budget in nwGOM coast

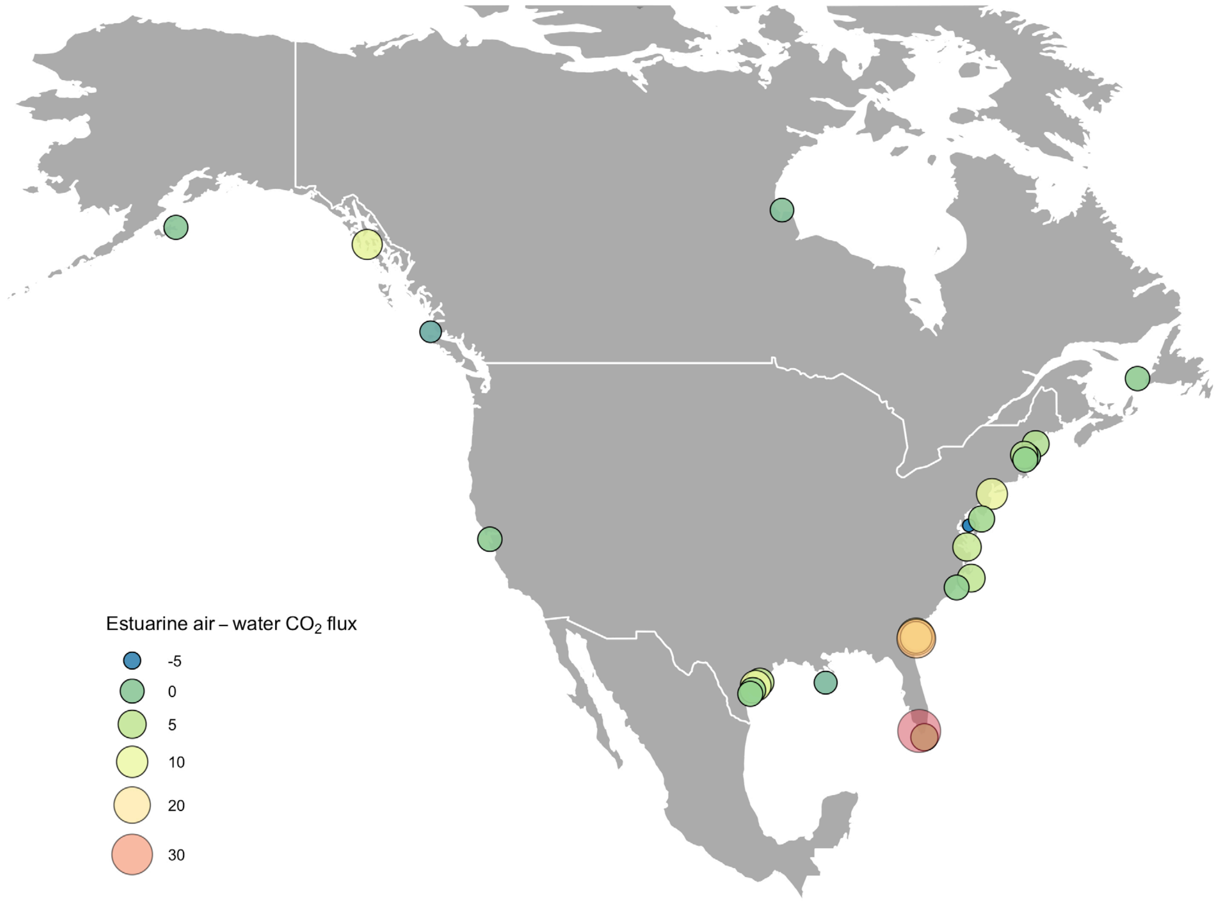

Figure 6. Observed estuarine air-water CO_2 fluxes in North America's coast. (unit: *mol·C·m*$^{-2}$*·yr*$^{-1}$, see details in Table **A6**)

The area-normalized annual estuarine CO_2 emission of the nwGOM coast was 4.0 ± 0.7 mol·C·m^{-2}·yr^{-1}, which was within the range of the area-normalized average CO_2 emission from the Atlantic coast (4.6 ± 1.9 mol·C·m^{-2}·yr^{-1}; Najjar et al., 2018) but almost two times of the entire North America coast average (~2.2 mol·C·m^{-2}·yr^{-1}; Chen et al., 2013). Moreover, area-normalized CO_2 emission in all GOM estuaries could reach 4.3 ± 4.8 mol·C·m^{-2}·yr^{-1} by integrating our observations and those in the literature (Table A6). This value was almost half of the arithmetic mean value from Windham-Myers et al. (2018), who found GOM estuarine CO_2

flux at an above average level (~8.1 mol·C·m^{-2}·yr^{-1}) among North American coasts. In addition, based on the arithmetic mean of our findings and existing observation-based F_{CO2}, the updated average of all North America estuarine CO_2 emission could reach 5.8 ± 9.0 mol·C·m^{-2}·yr^{-1} (Table A6). Note that tidal rivers were counted in those high estuarine CO_2 efflux regions (e.g., ~36.1 mol·C·m^{-2}·yr^{-1} in Shark River Estuary, Florida, Ho et al., 2016; ~25.3 mol·C·m^{-2}·yr^{-1} in Altamaha Sound, Georgia Coast, Jiang et al., 2008; Fig. 6). Nevertheless, given that previous syntheses of CO_2 fluxes were heavily skewed towards the Atlantic coastal estuaries (Chen et al., 2013; Najjar et al., 2018), our findings highlighted the diverse set of responses in different estuaries and the current lack of spatial coverage in estuarine CO_2 flux studies in general (Fig. 6).

Based on the current study and the literature, the relatively high estuarine CO_2 emissions are mostly in shallow (< 5 m) subtropical regions surrounded by extensive tidal wetlands (nwGOM, Florida Coast, Southern Atlantic Coast, Fig. 6; Table A6). One important reason for the high CO_2 flux was due to high riverine CO_2 in the southern U.S.A. ($p$$CO_2$ ranged 4000 – 6000 µatm; Butman and Raymond, 2011) or high wind speeds (Yao and Hu, 2017). Also lateral carbon exchange from saltmarshes and mangroves have not been adequately accounted for in explaining estuarine CO_2 flux. However, Windham-Myers et al. (2018) estimated a rate of 24.4 mol·C·m^{-2}·wetland·yr^{-1} for the nwGOM wetlands in terms of carbon sequestration, which is about ~6 times of the global average 4.8 mol·C·m^{-2}·wetland·yr^{-1} (Chmura et al., 2003). This, together with estimated estuarine carbon deposition rate found in the current study, could make nwGOM coast an important carbon storage region (also known as the "blue carbon", ~32.4 mol·C·m^{-2}·wetland·yr^{-1}, normalized to wetland area). Nevertheless, an improved re-evaluation of coastal carbon deposition is required, particularly with respect to future estuarine sedimentary carbon flux research to better constrain the rate of blue carbon conservation.

$F_{L\text{-}DIC}$ and $F_{L\text{-}TOC}$ contributed 62.7% and 86.5% of DIC and TOC inputs to nwGOM estuaries, respectively (Fig. 7). As a whole, ~36.5% of the DIC input was to support CO_2 emission and NEM, the remaining for oceanic export; yet on the TOC side, sediment deposition only accounted for about one-third of the total input, leaving ~70% for estuarine export. Therefore, carbon fluxes from nwGOM estuaries appear to largely depend on its extensive tidal wetlands.

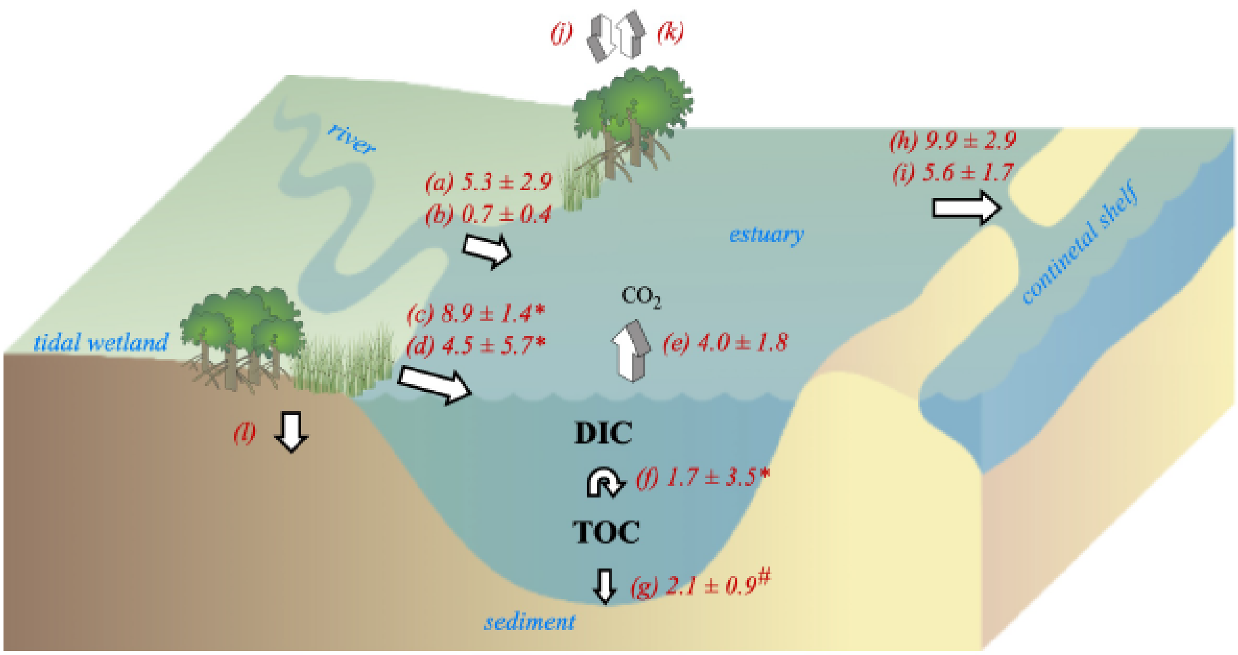

Figure 7. Schematic representation of integrated carbon fluxes in the nwGOM coast. (a) riverine DIC input; (b) riverine TOC input; (c) lateral DIC exchange between tidal wetlands and estuaries (d) lateral TOC exchange between tidal wetlands and estuaries; (e) air-water CO_2 flux; (f) pelagic and benthic NEM; (g) sediment TOC deposition; (h) DIC export to the open ocean; (i) TOC export to the open ocean; (j) carbon fixation by tidal wetland; (k) CO_2 evasion from tidal wetland; (l) carbon sequestration within tidal wetland. # denotes that the values are based on literature data; * denotes that the values are mainly dependent on other fluxes. (unit: $mol \cdot C \cdot m^{-2} \cdot yr^{-1}$)

4.4 Uncertainty

Integrating process-based fluxes could easily propagate the uncertainties. Uncertainty from each term was analyzed in Table A7. Note that we claimed a 100% uncertainty for both sedimentation rates and SGD, due to their high variabilities from literature data. Regardless, the carbon budget components showed a good agreement between total carbon loading and export

(Fig.7). Our estimated NEM from CO_2 flux displayed a range between -312.5 – 145.7 $mmol\cdot C\cdot m^{-2}\cdot d^{-1}$, similar to the finding in Russell and Montagna (2007), who estimated a NEM range of -250 – 187.5 $mmol\cdot C\cdot m^{-2}\cdot d^{-1}$ based on *in-situ* open water monitoring. However, even the direct NEM observations may suffer uncertainties from different methodologies (Gazeau et al., 2005). In addition, aggregated $F_{L\text{-}TOC}$ and $F_{L\text{-}DIC}$ were estimated at 4.5 ± 5.7 and 8.9 ± 1.4 $mol\cdot C\cdot m^{-2}\cdot yr^{-1}$, the fluxes could be further converted to wetland yields as 16.7 ± 21.4 and 33.5 ± 5.1 $mol\cdot C\cdot m^{-2}\cdot wetland\cdot yr^{-1}$ respectively. These values agreed with other tidal saltmarsh and mangrove systems as well (Table 2). However, direct measurement with sufficient spatiotemporal resolution is strongly recommended to confirm such crucial but varying carbon flux values.

5 Conclusions

The coastal carbon budget is important and highly dynamic. Our mass balance model indicated that lateral exchange from saltmarsh and mangrove habitats was a key driver to carbon budget in subtropical nwGOM lagoonal estuaries. For example, lateral TOC exchange could explain almost 86.5% of total TOC input into the estuary. On the other hand, the entire region served as an important CO_2 source to the atmosphere and at same time preserve considerable amount of blue carbon. The relatively high estuarine air-water CO_2 fluxes demonstrated the need for more extensive studies focusing on carbon cycling along the GOM coast to better constrain the North American coastal carbon budget, which is currently skewed toward the east coast.

Attempts to assess coastal carbon budget variability requires incorporation of estuarine hydrology. Our four-year dataset over various hydrologic conditions revealed as much as 2 – 10 times increase in estuarine CO_2 flux driven by floods compared with non-flooding (or dry) periods. However, the magnitude of change depended on estuarine residence time and the amount of freshwater inflow that each estuary received. Therefore, these estimates highlight the necessity of long-term regional focus to predict the future coastal carbon budget trajectories under changing hydrological conditions.

Appendices

The supporting information includes seven tables (Tables A1-A7), which provides more details on estuarine and riverine sampling schedules, parameters for F_{CO2} calculations, and a list of existing observation-based estuarine CO_2 fluxes from the North American coast. The information could be useful for those who are interested in seeing more details about how we collected and developed all flux terms on the nwGOM estuarine carbon budget.

Acknowledgements

We are grateful for the fieldwork assistance provided by the staff and students at both the Mission Aransas National Estuarine Research Reserve and Harte Research Institute at Texas A&M University-Corpus Christi. This study was funded by NOAA's NOS National Center for Coastal Ocean Science (Contract No. NA15NOS4780185), NSF Chemical Oceanography Program (OCE #1654232, OCE#1760006), and partly by the Guang Dong Basic and Applied Basic Research Foundation (Grant No. 2020A1515110828). This research was also supported in part by operations grants to the Mission-Aransas National Estuarine Research Reserve from NOAA's Office of Coastal Management. Data used in this study can be found in Biological and Chemical Oceanography Data Management Office (BCO-DMO) (Hu et al., 2019; McCutcheon and Hu, 2021). Dr. Chris Osburn and an anonymous reviewer provided critical evaluation that helped to improve the quality of the manuscript.

Reference

An, S., and Joye, S. B. (2001). Enhancement of coupled nitrification-denitrification by benthic photosynthesis in shallow estuarine sediments. Limnology and Oceanography, 46(1), 62-74.

Akhand, A., Watanabe, K., Chanda, A., Tokoro, T., Chakraborty, K., Moki, H., Tanaya, T., Ghosh, J. and Kuwae, T. (2021). Lateral carbon fluxes and CO_2 evasion from a subtropical mangrove-seagrass-coral continuum. Science of The Total Environment 752, 142190.

Bauer, J. E., Cai, W. J., Raymond, P. A., Bianchi, T. S., Hopkinson, C. S., and Regnier, P. A. (2013). The changing carbon cycle of the coastal ocean. Nature, 504(7478), 61-70.

Benway, H., and Coble, P. (2014). Report of The US Gulf of Mexico Carbon Cycle Synthesis Workshop, March 27-28, 2013. Ocean Carbon and Biogeochemistry Program and North American Carbon Program.

Bianchi, T. S., Pennock, J. R., and Twilley, R. R. (1999). Biogeochemistry of Gulf of Mexico estuaries: John Wiley & Sons.

Bianchi, T. S., Allison, M. A., Zhao, J., Li, X., Comeaux, R. S., Feagin, R. A., Kulawardhana, R. W. (2013). Historical reconstruction of mangrove expansion in the Gulf of Mexico: linking climate change with carbon sequestration in coastal wetlands. Estuarine, Coastal and Shelf Science, 119, 7-16.

Bogard, M.J., Bergamaschi, B.A., Butman, D.E., Anderson, F., Knox, S.H. and Windham-Myers, L. (2020). Hydrologic Export Is a Major Component of Coastal Wetland Carbon Budgets. Global Biogeochemical Cycles 34(8), e2019GB006430.

Bouillon, S., Borges, A. V., Castañeda-Moya, E., Diele, K., Dittmar, T., Duke, N. C., et al. (2008). Mangrove production and carbon sinks: a revision of global budget estimates. Global Biogeochemical Cycles, 22(2).

Bronikowski, J. L. (2004). Sedimentary environments and processes in a shallow, Gulf Coast Estuary-Lavaca Bay, Texas. Texas A&M University,

Butman, D., and Raymond, P. A. (2011). Significant efflux of carbon dioxide from streams and rivers in the United States. Nature Geoscience, 4(12), 839-842.

Cai, W. J. (2011). Estuarine and coastal ocean carbon paradox: CO_2 sinks or sites of terrestrial carbon incineration? Annual review of marine science, 3, 123-145.

Chen, C. T. A., Huang, T. H., Chen, Y. C., Bai, Y., He, X., and Kang, Y. (2013). Air–sea exchanges of CO_2 in the world's coastal seas. Biogeosciences, 10(10), 6509-6544.

Chen, X., Zhang, F., Lao, Y., Wang, X., Du, J. and Santos, I.R. (2018). Submarine Groundwater Discharge-Derived Carbon Fluxes in Mangroves: An Important Component of Blue Carbon Budgets? Journal of Geophysical Research: Oceans 123(9), 6962-6979.

Chmura, G. L., Anisfeld, S. C., Cahoon, D. R., and Lynch, J. C. (2003). Global carbon sequestration in tidal, saline wetland soils. Global Biogeochemical Cycles, 17(4).

Crosswell, J. R., Anderson, I. C., Stanhope, J. W., Van Dam, B., Brush, M. J., Ensign, S., et al. (2017). Carbon budget of a shallow, lagoonal estuary: Transformations and source-sink dynamics along the river-estuary-ocean continuum. Limnology and Oceanography, 62, S29-S45.

Crosswell, J. R., Wetz, M. S., Hales, B., and Paerl, H. W. (2014). Extensive CO_2 emissions from shallow coastal waters during passage of Hurricane Irene (August 2011) over the Mid-Atlantic coast of the U.S.A. Limnology and Oceanography, 59(5), 1651-1665.

Dürr, H. H., Laruelle, G. G., van Kempen, C. M., Slomp, C. P., Meybeck, M., and Middelkoop, H. (2011). Worldwide typology of nearshore coastal systems: Defining the estuarine filter of river inputs to the oceans. Estuaries and Coasts, 34(3), 441-458.

Gazeau, F., Borges, A.V., Barrón, C., Duarte, C.M., Iversen, N., Middelburg, J.J., Delille, B., Pizay, M.-D., Frankignoulle, M. and Gattuso, J.-P. (2005). Net ecosystem metabolism in a micro-tidal estuary (Randers Fjord, Denmark): evaluation of methods. Marine Ecology Progress Series 301, 23-41.

Gordon, D., Boudreau, P., Mann, K., Ong, J., Silvert, W., Smith, S., et al. (1996). LOICZ biogeochemical modelling guidelines (Vol. 5): LOICZ Core Project, Netherlands Institute for Sea Research Yerseke.

Herrmann, M., Najjar, R. G., Kemp, W. M., Alexander, R. B., Boyer, E. W., Cai, W.-J., . . . Smith, R. A. (2015). Net ecosystem production and organic carbon balance of U.S. East Coast estuaries: A synthesis approach. Global Biogeochemical Cycles, 29(1), 96-111.

Ho, D. T., Coffineau, N., Hickman, B., Chow, N., Koffman, T., and Schlosser, P. (2016). Influence of current velocity and wind speed on air-water gas exchange in a mangrove estuary. Geophysical Research Letters, 43(8), 3813-3821.

Hopkinson, C. S. (1988). Patterns of organic carbon exchange between coastal ecosystems. In Coastal-Offshore Ecosystem Interactions (Vol. 22, pp. 122-154). Berlin, Heidelberg: Springer.

Hu, X. (2019) Carbonate chemistry effects from Hurricane Harvey in San Antonio Bay and Mission Aransas Estuary from 2017-02-22 to 2018-11-15. Biological and Chemical Oceanography Data Management Office (BCO-DMO). (Version 1) Version Date 2019-12-19.

Hu, X., Yao, H., Staryk, C. J., McCutcheon, M. R., Wetz, M. S., and Walker, L. (2020). Disparate responses of carbonate system in two adjacent subtropical estuaries to the influence of Hurricane Harvey – A case study. Frontiers in Marine Science, 7(26).

Jiang, L. Q., Cai, W. J., and Wang, Y. (2008). A comparative study of carbon dioxide degassing in river- and marine-dominated estuaries. Limnology and Oceanography, 53(6), 2603-2615.

Kemp, W., Smith, E., Marvin-DiPasquale, M., and Boynton, W. (1997). Organic carbon balance and net ecosystem metabolism in Chesapeake Bay. MARINE ECOLOGY PROGRESS SERIES, 229-248.

Laruelle, G. G., Dürr, H. H., Lauerwald, R., Hartmann, J., Slomp, C. P., Goossens, N., and Regnier, P. A. G. (2013). Global multi-scale segmentation of continental and coastal waters from the watersheds to the continental margins. Hydrology and Earth System Sciences, 17(5), 2029-2051.

Liu, N., Liu, C. and Lavigne, T. (2019). The Variation of the Intensity, Height, and Size of Precipitation Systems with El Niño–Southern Oscillation in the Tropics and Subtropics. Journal of Climate 32(14), 4281-4297.

Maher, D. T., Call, M., Santos, I. R., and Sanders, C. J. (2018). Beyond burial: lateral exchange is a significant atmospheric carbon sink in mangrove forests. Biology Letters, 14(7), 20180200.

Maher, D. T., and Eyre, B. D. (2012). Carbon budgets for three autotrophic Australian estuaries: Implications for global estimates of the coastal air-water CO_2 flux. Global Biogeochemical Cycles, 26(1).

Mitra, S., Osburn, C.L. and Wozniak, A.S. (2017). A Preliminary Assessment of Fossil Fuel and Terrigenous Influences to Rainwater Organic Matter in Summertime in the Northern Gulf of Mexico. Aquatic Geochemistry 23(4), 217-231.

McCutcheon, M. R., Hu, X. (2021) Carbonate chemistry in Mission Aransas Estuary from May 2014 to Feb 2017 and Dec 2018 to Feb 2020. Biological and Chemical Oceanography Data Management Office (BCO-DMO). (Version 1) Version Date 2021-01-04.

McCutcheon, M.R., Yao, H., Staryk, C.J. and Hu, X. (2021). Temporal variability and driving factors of the carbonate system in the Aransas Ship Channel, TX, USA: a time series study. Biogeosciences 18(15), 4571-4586.

Millero, F. J. (2010). Carbonate constants for estuarine waters. Marine and Freshwater Research, 61, 139-142.

Montagna, P.A., Brenner, J., Gibeaut, j., and Morehead, S. (2011). Coastal Impacts. In: Schmandt, J., G.R. North, and J. Clarkson (eds.), The Impact of Global Warming on Texas, second edition. University of Texas Press, Austin, Texas, pp. 96-123.

Montagna, P., Palmer, T. A., and Pollack, J. (2013). Hydrological Changes and Estuarine Dynamics: Springer Briefs in Environmental Sciences, New York, New York.

Montagna, P. A., and Kalke, R. D. (1992). The effect of freshwater inflow on meiofaunal and macrofaunal populations in the Guadalupe and Nueces estuaries, Texas. Estuaries, 15(3), 307-326.

Murgulet, D., Trevino, M., Douglas, A., Spalt, N., Hu, X., and Murgulet, V. (2018). Temporal and spatial fluctuations of groundwater-derived alkalinity fluxes to a semiarid coastal embayment. Science of the Total Environment, 630, 1343-1359.

Najjar, R. G., Herrmann, M., Alexander, R., Boyer, E. W., Burdige, D. J., Butman, D., et al. (2018). Carbon budget of tidal wetlands, estuaries, and shelf waters of eastern North America. Global Biogeochemical Cycles, 32(3), 389-416.

Orr, J. C., Epitalon, J.-M., Dickson, A. G., and Gattuso, J.-P. (2018). Routine uncertainty propagation for the marine carbon dioxide system. Marine Chemistry, 207, 84-107.

Paerl, H.W., Crosswell, J.R., Van Dam, B., Hall, N.S., Rossignol, K.L., Osburn, C.L., Hounshell, A.G., Sloup, R.S. and Harding, L.W. (2018). Two decades of tropical cyclone impacts on North Carolina's estuarine carbon, nutrient and phytoplankton dynamics: implications for biogeochemical cycling and water quality in a stormier world. Biogeochemistry 141(3), 307-332.

Ravichandran, M., M. Baskaran, P. H. Santschi, and T. S. Bianchi (1995), Geochronology of sediments in the Sabine-Neches estuary, Texas, U.S.A, Chemical Geology, 125(3), 291-306.

Roth, D (2010) Texas Hurricane History (National Weather Service, Camp Springs, MD).

Russell, M. J., and Montagna, P. A. (2007). Spatial and temporal variability and drivers of net ecosystem metabolism in western Gulf of Mexico estuaries. Estuaries and Coasts, 30(1), 137-153.

Russell, M. J., Montagna, P. A., and Kalke, R. D. (2006). The effect of freshwater inflow on net ecosystem metabolism in Lavaca Bay, Texas. Estuarine, Coastal and Shelf Science, 68(1-2), 231-244.

Santos, I. R., Maher, D. T., Larkin, R., Webb, J. R., and Sanders, C. J. (2019). Carbon outwelling and outgassing vs. burial in an estuarine tidal creek surrounded by mangrove and saltmarsh wetlands. Limnology and Oceanography, 64(3), 996-1013.

Santos, I.R., Burdige, D.J., Jennerjahn, T.C., Bouillon, S., Cabral, A., Serrano, O., Wernberg, T., Filbee-Dexter, K., Guimond, J.A. and Tamborski, J.J. (2021). The renaissance of Odum's outwelling hypothesis in 'Blue Carbon' science. Estuarine, Coastal and Shelf Science 255, 107361.

Santschi, P. H., B. J. Presley, T. L. Wade, B. Garcia-Romero, and M. Baskaran (2001), Historical contamination of PAHs, PCBs, DDTs, and heavy metals in Mississippi River Delta, Galveston Bay and Tampa Bay sediment cores, Marine Environmental Research, 52(1), 51-79.

Sherwood, S. and Fu, Q. (2014). A Drier Future? Science 343(6172), 737-739.

Sippo, J. Z., Maher, D. T., Tait, D. R., Holloway, C., and Santos, I. R. (2016). Are mangroves drivers or buffers of coastal acidification? Insights from alkalinity and dissolved inorganic carbon export estimates across a latitudinal transect. Global Biogeochemical Cycles, 30(5), 753-766.

Smith, S., Buddemeier, R., Wulff, F., Swaney, D., Camacho-Ibar, V., David, L., . . . McLaughlin, C. (2005). C, N, P fluxes in the coastal zone. In C.J. Crossland, H.H. Kremer, H.J. Lindeboom, J.I. Marshall Crossland, & M. D. A. L. Tissier (Eds.), Coastal Fluxes in the Anthropocene (pp. 95-143): Springer.

Smith, S. V., Hollibaugh, J. T., Dollar, S. J., and Vink, S. (1991). Tomales Bay metabolism: C-N-P stoichiometry and ecosystem heterotrophy at the land-sea interface. Estuarine, Coastal and Shelf Science, 33(3), 223-257.

Solis, R., and Powell, G. (1999). Hydrography, mixing characteristics, and residence times of Gulf of Mexico estuaries. In Biogeochemistry of Gulf of Mexico estuaries (pp. 29-61): John Wiley & Sons.

Spalt, N., Murgulet, D., and Abdulla, H. (2020). Spatial variation and availability of nutrients at an oyster reef in relation to submarine groundwater discharge. Science of the Total Environment, 710, 136283.

Spruill, T. B., and J. F. Bratton (2008), Estimation of groundwater and nutrient fluxes to the Neuse River Estuary, North Carolina, Estuaries and Coasts, 31(3), 501-520.

Stets, E.G., Kelly, V.J., and Crawford, C.G. (2014). Long-term trends in alkalinity in large rivers of the conterminous US in relation to acidification, agriculture, and hydrologic modification. Science of The Total Environment, 488–489, 280-289.

Swaney, D. P., Humborg, C., Emeis, K., Kannen, A., Silvert, W., Tett, P., et al. (2012). Five critical questions of scale for the coastal zone. Estuarine, Coastal and Shelf Science, 96, 9-21.

Tamborski, J.J., Eagle, M., Kurylyk, B.L., Kroeger, K.D., Wang, Z.A., Henderson, P. and Charette, M.A. (2021). Pore water exchange-driven inorganic carbon export from intertidal salt marshes. Limnology and Oceanography 66(5), 1774-1792.

Tanner, E. L., and Eyre, B. D. (2020). Carbon Budget for a Large Drowned River Valley Estuary Adjacent to an Emerging Megacity (Sydney Harbour). Journal of Geophysical Research: Biogeosciences, 125(1).

Van Dam, B. R., Crosswell, J. R., and Paerl, H. W. (2018). Flood-driven CO_2 emissions from adjacent North Carolina estuaries during Hurricane Joaquin (2015). Marine Chemistry, 207, 1-12.

Walker, L. M., Montagna, P.A., Hu, X., Wetz, M.S. (2021). Timescales and magnitude of water quality change in three Texas estuaries induced by passage of Hurricane Harvey. Estuaries and Coasts, 44(2), 460-971. https://doi.org/10.1007/s12237-020-00846-6

Wang, Z. A., Kroeger, K. D., Ganju, N. K., Gonneea, M. E., and Chu, S. N. (2016). Intertidal salt marshes as an important source of inorganic carbon to the coastal ocean. Limnology and Oceanography, 61(5), 1916-1931.

Weiss, R. F., and Price, B. A. (1980). Nitrous oxide solubility in water and seawater. Marine Chemistry, 8, 347-359.

Weiss, R. F. (1974). Carbon dioxide in water and seawater: the solubility of a non-ideal gas. Marine Chemistry, 2(3), 203-215.

Willey, J. D., Kieber, R. J., Eyman, M. S., and Avery, G. B. (2000). Rainwater dissolved organic carbon: concentrations and global flux. Global Biogeochemical Cycles, 14(1), 139-148.

Windham-Myers, L., Wei Jun, C., Simone, A., Andreas, A., Joseph, C., Kenneth, D., . . . Maria, T. (2018). Chapter 15: Tidal Wetlands and Estuaries. In N. Cavallaro, G. Shrestha, R. Birdsey, M. A. Mayes, R. G. Najjar, S. C. Reed, P. Romero-Lankao, and Z. Zhu (Eds.), Second State of the Carbon Cycle Report (SOCCR2): A Sustained Assessment Report. U.S. Global Change Research Program (pp. 596-648). Washington D.C., USA.

Yao, H., and Hu, X. (2017). Responses of carbonate system and CO_2 flux to extended drought and intense flooding in a semiarid subtropical estuary. Limnology and Oceanography, 62, S112-S130.

Yao, H., McCutcheon, M.R., Staryk, C.J. and Hu, X. (2020). Hydrologic controls on CO2 chemistry and flux in subtropical lagoonal estuaries of the northwestern Gulf of Mexico. Limnology and Oceanography 65(6), 1380-1398.

Yeager, K. M., Santschi, P., Schindler, K., Andres, M., and Weaver, E. (2006). The relative importance of terrestrial versus marine sediment sources to the Nueces-Corpus Christi Estuary, Texas: An isotopic approach. Estuaries and Coasts, 29(3), 443-454.

Zeng, F.-W., Masiello, C. A., and Hockaday, W. C. (2011). Controls on the origin and cycling of riverine dissolved inorganic carbon in the Brazos River, Texas. Biogeochemistry, 104(1-3), 275-291.

Table 1. Hydrologic and sedimentary information for four nwGOM lagoonal estuaries

Characteristic		Location				Reference
		LCE	GE	MAE	NE	
Mean Depth (m)		1.1	1.1	1.1	1.2	(Solis and Powell, 1999)
Open Water Area (km^2)		1180.6	561.6	575.7	536.6	(TCEQ)
Watershed Area ($10^3 \cdot km^2$)		130.3	28.1	7.2	45.6	(Montagna et al., 2011)
Residence Time (d)		81	39	360	356	(Bianchi et al., 1999)
Submarine Groundwater Discharge ($m \cdot d^{-1}$)		0.46[a] (0.11)	0.46[a] (0.11)	0.46 (0.11)	1.08 (0.18)	(Murgulet et al., 2018; Spalt et al., 2020)
River Discharge ($m^3 \cdot s^{-1}$)	A	107.9 (137.8)	48.3 (24.8)	7.3 (13.4)	8.6 (16.9)	(USGS, gauge#8162600, 8162000, 8162500, 8164600, 8164800, 8164000, 8188810, 8189800, 8189200, 8189500, 8189700, 8211200, 8211520)
	D	30.0 (16.2)	28.3 (12.0)	0.9 (1.1)	3.0 (1.2)	
	W	273.5 (162.8)	72.5 (16.8)	32.0 (14.4)	23.7 (31.8)	
Riverine DIC ($\mu mol \cdot kg^{-1}$)	D	2941.9 (569.6)	4454.9 (535.0)	4948.4 (994.4)	4062.6 (297.4)	(This study)
	W	2061.2 (879.6)	2884.6 (758.5)	2925.7 (957.4)	3744.5 (388.9)	
Riverine TOC ($\mu mol \cdot kg^{-1}$)	D	558.4 (204.9)	371.5 (151.4)	300.7 (31.1)	619.3 (72.9)	(TCEQ)
	W	368.7 (242.6)	558.6 (333.4)	777.2 (221.0)	605.9 (125.6)	
Ocean endmember ($\mu mol \cdot kg^{-1}$)	D	DIC:	2232.3 (69.6)	TOC	166.7	(TCEQ)
	W	DIC	2094.9 (65.2)	TOC	166.7	
Surface sediment TOC ($g \cdot C \cdot kg^{-1}$)	D	5.4 (3.7)	6.0 (0.8)	2.8 (0.7)	4.2 (1.8)	(TCEQ)
	W	10.6 (8.1)	9.8 (5.3)	21.4 (15.9)	5.2 (3.3)	
Sediment accumulation rate[b] ($cm \cdot yr^{-1}$)	Upper	0.79 (0.37)	0.79[c] (0.37)	0.43[c] (0.12)	0.43 (0.12)	(Bronikowski, 2004; Yeager et al., 2006)
	Lower	0.23[3] (0.05)	n/a	0.23[3] (0.05)	0.23 (0.05)	
Bulk density	0.88 $g \cdot cm^{-3}$; averaged from nearby nwGOM estuary studies: Galveston Bay (Santschi et al., 2001) and Sabine Lake (Ravichandran et al., 1995), data collected by Hutchings et al. (2020).					

Values in parentheses indicate the standard errors.
A=annual average, D=dry condition, including dry and flood relaxation periods, W=wet condition, including flooding and hurricane periods;
TCEQ=Texas Commission of Environmental Quality, Texas Surface Water Quality Monitoring, https://www.tceq.texas.gov/;
[a] Assume that SGD in LCE and GE were similar as MAE due to a lack of study;
[b] Sediment accumulation rate was based on the ^{210}Pb methodology;
[c] Assume the same sediment accumulation rates for upper LCE/GE and upper MAE/NE, all lower estuaries were assumed to have the same sediment accumulation rate due to their hydrologic similarities.

Table 2. Recorded lateral TOC and DIC exchanges yielded from saltmarsh and mangrove habitats (*units*: $mol \cdot C \cdot m^{-2} \cdot wetland \cdot yr^{-1}$).

Region	Wetland System	Surface Area (km^2)	Lateral TOC	Lateral DIC	Reference
Global	Mangrove	1.6×10^5	21.0 (23.1)	-	(Bouillon et al., 2008)
U.S. East Coast	Salt Marsh	1.23×10^4	14.9	34.6	(Wang et al., 2016)
U.S. East Coast	Salt Marsh and Mangrove	1.02×10^4	15.4 (5.9)		(Herrmann et al., 2015)
U.S. East Coast	Salt Marsh And Mangrove	1.02×10^4		19.6 (10.0)	(Najjar et al., 2018)
Maowei Sea (China)	Mangrove	135	102.2 (15.5)	177.0 (121.3)	(Chen et al., 2018)
Iriomote Island (Japan)	Mangrove	0.22	3.4	11.9	(Akhand et al., 2021)
Southern Moreton Bay (Australia)	Mangrove		20.0 (4.7)	34.2 (12.0)	(Maher et al., 2018)
Australian Coast	Mangrove	8.12	-	21.5 (10.6)	(Sippo et al., 2016)
nwGOM (U.S.)	Salt Marsh and Mangrove	571.5*	16.7 (21.4)	33.5 (5.1)	This study

Values in parentheses indicate standard errors;
*Value was measured based on Google Earth software.